Conference paper

Ana M. Matos[a], Joana S. Cristóvão[a], Dmitry V. Yashunsky, Nikolay E. Nifantiev, Ana S. Viana, Cláudio M. Gomes* and Amélia P. Rauter*

Synthesis and effects of flavonoid structure variation on amyloid-β aggregation

DOI 10.1515/pac-2017-0201

Abstract: Dietary flavonoids and synthetic derivatives have a well-known potential for biomedical applications. In this perspective, we report herein new methodologies to access chrysin and 5,7-dihydroxychromone, and these structures were combined with those of naturally occurring quercetin, luteolin, (+)-dihydroquercetin and apigenin to assemble a set of polyphenols with structure variations for in vitro testing over the aggregation of Alzheimer's disease (AD) amyloid peptide $A\beta_{1-42}$. Using thioflavin-T (ThT) monitored kinetics and subsequent mechanistic analysis by curve fitting, we show that catechol-type flavonoids reduce $A\beta_{1-42}$ fibril content by 30 % at molar ratios over 10. Without affecting secondary nucleation, these compounds accelerate primary nucleation events responsible for early primary oligomer formation, putatively redirecting the latter into off-pathway aggregates. Atomic force microscopy (AFM) imaging of reaction end-points allowed a comprehensive topographical analysis of amyloid aggregate populations formed in the presence of each compound. Formation of $A\beta_{1-42}$ small oligomers, regarded as the most toxic amyloid structures, seems to be limited by flavonoids with a C2 phenyl group, while flavonol 3-OH is not a beneficial structural feature. Overall, the diversity of structural variations within flavonoids opens avenues for their development as chemical tools in the treatment of AD by tackling the formation and distribution of neurotoxic oligomers species.

Keywords: amyloid-β aggregation kinetics; atomic force microscopy; chemical synthesis; flavonoids; ICS-28; ThT fluorescence assay.

Article note: A collection of invited papers based on presentations at the XXVIII International Carbohydrate Symposium (ICS-28), New Orleans, July 17–21, 2016.

[a]**Ana M. Matos and Joana S. Cristóvão:** These authors contributed equally to this work.
***Corresponding authors: Cláudio M. Gomes,** Biosystems and Integrative Sciences Institute, Faculdade de Ciências, Universidade de Lisboa, and Departamento de Química e Bioquímica, Faculdade de Ciências, Universidade de Lisboa, Campo Grande, 1749-016 Lisboa, Portugal, e-mail: cmgomes@fc.ul.pt; and **Amélia P. Rauter,** Centro de Química e Bioquímica, Faculdade de Ciências, Universidade de Lisboa and Departamento de Química e Bioquímica, Faculdade de Ciências, Universidade de Lisboa, Ed. C8, Campo Grande, 1749-016 Lisboa, Portugal, e-mail: aprauter@fc.ul.pt
Ana M. Matos: Centro de Química e Bioquímica, Faculdade de Ciências, Universidade de Lisboa and Departamento de Química e Bioquímica, Faculdade de Ciências, Universidade de Lisboa, Ed. C8, Campo Grande, 1749-016 Lisboa, Portugal; and CEDOC Chronic Diseases, Nova Medical School, Rua Câmara Pestana n° 6, 6-A, CEDOC II, 1150-082, Lisboa, Portugal
Joana S. Cristóvão: Biosystems and Integrative Sciences Institute, Faculdade de Ciências, Universidade de Lisboa, 1749-016 Lisboa; and Departamento de Química e Bioquímica, Faculdade de Ciências, Universidade de Lisboa, Campo Grande, 1749-016 Lisboa, Portugal
Dmitry V. Yashunsky and Nikolay E. Nifantiev: Laboratory of Glycoconjugate Chemistry, N. D. Zelinsky Institute of Organic Chemistry, Russian Academy of Sciences, Leninsky, Prospect 47, 119991 Moscow, Russian Federation
Ana S. Viana: Centro de Química e Bioquímica, Faculdade de Ciências, Universidade de Lisboa and Departamento de Química e Bioquímica, Faculdade de Ciências, Universidade de Lisboa, Ed. C8, Campo Grande, 1749-016 Lisboa, Portugal

Introduction

Being accountable for 60–80 % of all cases of senile dementia, (AD) currently affects more than 46 million people worldwide and typically manifests with progressive memory loss and cognitive decline [1]. While the pathophysiological mechanisms leading to these symptoms are not fully clarified yet, it is widely agreed that brain accumulation of Aβ aggregates into plaques and neurofibrillary tangles containing hyperphosphorylated tau are largely involved in triggering brain oxidative stress and neuroinflammatory events that ultimately result in synaptic dysfunction and neuronal death [2].

In addition to the well-known genetic risk factors associated to sporadic AD such as the type 2 diabetes-related apolipoprotein E-ε4 allele, altered expression or activity of Aβ precursor protein cleaving enzyme β secretase enzyme-1 is also pointed out as a cause for oversecretion of Aβ peptides in the brain in late-onset cases [2]. A number of aggregation prone Aβ peptides is then formed, of which the notoriously more toxic one is the $A\beta_{1-42}$ variant. There is also growing evidence indicating that chronic inflammation associated with hyperinsulinemia and persistent infections typically found in immune-senescent old adults should be regarded as a major factor contributing to the increasing incidence of AD [2–4]. Interestingly, circulating islet amyloid polypeptide oversecreted by pancreatic β-cells in hyperinsulinemic states promotes heterologous seeding with Aβ to form amyloid aggregates in the cerebrovascular structure and brain parenchyma of type 2 diabetic patients [5]. On the other hand, Aβ has been recently shown to have a dual injuring and protective role against microbial infectious agents in the brain: after forming soluble oligomers, it binds to glycans that are present in the surface of bacterial cell walls through a heparin-binding domain, thus preventing their interaction and adhesion to the host cell [6]. Accordingly, bacterial molecules were found to colocalize with Aβ amyloid plaques and around vessels of diseased brains [7].

Mechanistically, $A\beta_{1-42}$ peptide undergoes a highly complex but relatively well described self-aggregation pathway in the brain, initially involving a primary nucleation phase to form primary fibrils that grow longer in the subsequent elongation process. These fibrils then catalyze secondary nucleation events by recruiting soluble monomers to form cytotoxic oligomeric species, which are able to further multiply themselves in a positive feedback loop [8–10], as illustrated in Fig. 1. This self-assembly reaction also involves the generation of off-pathway aggregates arising from the main fibril assembly route, which are generally more amorphous and frequently stable final reaction end-points, rather than intermediates. Together, these events account for the polymorphism of β-amyloid species found in the sequence of the self-assembly process of $A\beta_{1-42}$ monomers. Yet, it has been shown in vivo that close to amyloid plaques the secondary nucleation process is significantly enhanced when compared to primary nucleation events and, although amyloid fibrils do not seem to be the major cause of direct neurotoxicity, once they are present in a small

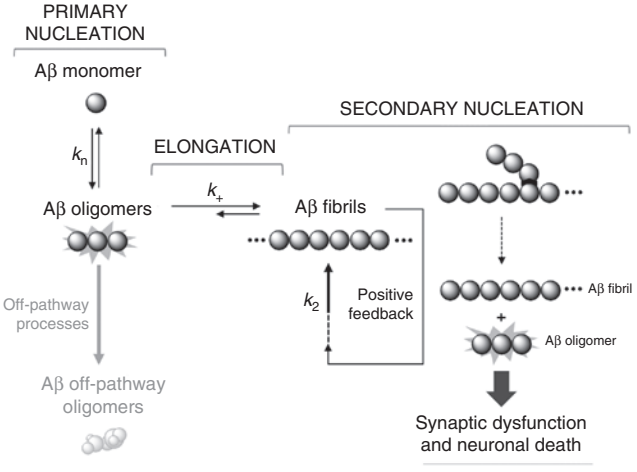

Fig. 1: Simplified representation of the Aβ aggregation pathway. k_n, primary nucleation rate; k_+, elongation rate; k_2, secondary nucleation rate [adapted from reference 10].

but critical concentration, they are indeed the major source of new diffusible cytotoxic oligomers by surface catalysis [8, 10]. Hence, by tackling secondary nucleation in addition to the primary nucleation process, the proliferation of neurotoxic Aβ oligomers could be prevented [10, 11].

Dietary flavonoids have been extensively studied for a variety of medical applications, and many of them were shown to display advantageous neuroprotective properties associated with multitarget mechanisms of action. Indeed, different flavonoids as natural phenolic compounds exhibit very high antioxidant effect [12, 13], but (+)-dihydroquercetin (**3**) was shown to have potential to ameliorate the serious consequences of acute and chronic traumata of the mammalian nervous system [14], while quercetin (**1**) and luteolin (**2**) are potent antioxidant and anti-inflammatory molecules with activity against Aβ-induced neurotoxicity, anti-amyloidogenic and fibril-disaggregating effects, being additionally able to regulate BACE1-mediated AβPP processing [15–21]. Moreover, both catechol-type flavonoids were shown to have therapeutic potential in the treatment of insulin resistance and bacterial infections in vivo [22, 23], which encourages further optimization of the flavonoid scaffold to tackle diabetes- and microbe-induced Aβ accumulation and neurotoxicity. Yet, a non-catechol-type flavone, chrysin (**5**), has also been described as a potent neuroprotective agent able to reduce Aβ-induced oxidative stress, neuroinflammation and hippocampal neuronal loss, resulting in the prevention of cognitive decline [24–26]. This compound can also tackle vascular complications associated with insulin resistance [27] and has recently served as scaffold for the development of new β-ketoacyl-acyl carrier protein synthase III (FabH) inhibitors with antimicrobial activity [28]. Indeed, these data suggest that the catechol group in the flavonoid scaffold might not be a "must have" moiety in the design of new multitarget flavonoid-based compounds with neuroprotective activity.

Although active, natural flavonoids usually display low oral bioavailability and poor metabolic stability due to rapid conjugation with glucuronic acid or sulphate groups [29]. In order to rationally design and synthesize new molecules with potential to interfere with Aβ aggregation and improved selectivity and pharmacokinetic properties, we were interested in identifying critical flavonoid structural features required for activity over amyloid aggregation. By conducting an analysis of structure-activity relationships with the naturally occurring pentahydroxyflavone quercetin (**1**), the tetra- and tri-hydroxyflavones, respectively luteolin (**2**) and apigenin (**4**) (Fig. 2), the hydroxylation pattern in flavones is studied, while comparison with the pentahydroxyflavan-4-one (**3**) may give insights into the relevance of the alkene for the bioactivity. Synthesis of the dihydroxyflavone chrysin (**5**) and that of 5,7-dihydroxychromone (**6**) was undertaken by new methodologies (Scheme 1), aiming to evaluate if flavonoid ring B is required for activity. By carrying out this research, our main goal is to elicit the chemical core structure that might account for the anti-amyloid aggregation activity of the studied flavonoids, aiming to establish a lead scaffold for further development.

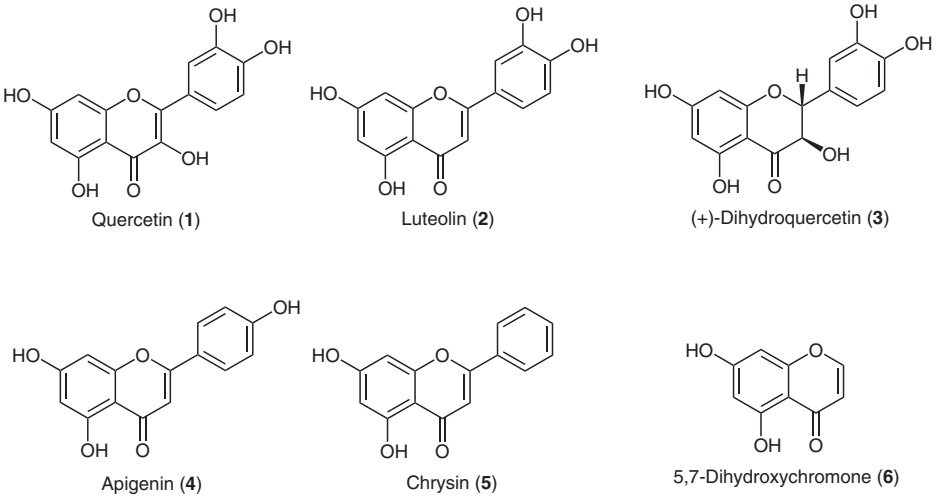

Fig. 2: Dietary flavonoids with potential to inhibit $A\beta_{1-42}$ fibrillization used in this study: the flavonol quercetin (**1**), the 3-hydroxyflavanone (+)-dihydroquercetin (**3**), three flavones – luteolin (**2**), apigenin (**4**) and chrysin (**5**), and the 5,7-dihydroxychromone (**6**).

Experimental section

General experimental procedures

HPLC grade solvents and reagents were obtained from commercial suppliers and were used without further purification. LCMS experiments were performed in a column XBridge C18 3.5u 2.1×50 mm at 1.2 mL/min and 50 °C; 10 mM ammonium bicarbonate pH 9/ACN, gradient 10 > 95 % ACN in 1.5 min + 0.5 min hold. Flash column chromatography was performed using CombiFlash® Rf200 (Teledyne Isco). Preparative HPLC was performed in a Gilson apparatus using either Phenomenex gemini NX, C18, 5 µm 30×100 mm or Phenomenex gemini NX, C18, 10 µm 50×150 mm columns. NMR spectra were recorded on a Bruker AV III HD Nanobay spectrometer running at 400.13 MHz equipped with a room temperature 5 mm BBO Smartprobe with Z-gradients capable of ^{19}F observation. Chemical shifts are expressed in δ (ppm) and the proton coupling constants *J* in hertz (Hz). NMR data were assigned using appropriate COSY, DEPT, HMQC, and HMBC spectra. Melting points were measured using a Stuart SMP30 melting point apparatus. Tested compounds have ≥95 % purity as determined by LCMS.

Preparation of 1-[2-hydroxy-4,6-bis(methoxymethoxy)phenyl]ethan-1-one (8)

2,4,6-Trihydroxyacetophenone monohydrate (2.0 g, 10.74 mmol) was dissolved in acetone (40 mL), then potassium carbonate (3.12 g, 22.56 mmol, 2.1 eq.) was slowly added at room temperature and the mixture was stirred for 5 min. Chloromethyl methyl ether (1.72 mL, 22.56 mmol, 2.1 eq.) was then added in a dropwise manner. The temperature was raised to 56 °C and the reaction was followed by LCMS. After stirring for 2 h, the reaction has reached completion (52 % reaction yield). The mixture was then cooled to room temperature, poured into water and extracted with DCM (3×50 mL). The organic layers were combined, dried over magnesium sulphate, filtered-off, and concentrated under vacuum. The residue was purified by column chromatography (isohexane/ethyl acetate 3:2) to afford the desired product **8** as colourless oil. ^{1}H NMR ($CDCl_3$) δ 13.71 (1H, s, OH-2), 6.27 (1H, d, J_{meta} = 2.29 Hz, H-5), 6.25 (1H, d, J_{meta} = 2.30 Hz, H-3), 5.26 (2H, s, −OCH_2O−), 5.17 (2H, s, −OCH_2O−), 3.52 (3H, s, −OCH_3), 3.47 (3H, s, −OCH_3), 2.66 (3H, s, CH_3−Ac); ^{13}C NMR δ 203.2 (C=O), 166.8 (C-2), 163.5 (C-4), 160.4 (C-6), 107.0 (C-1), 97.2 (C-3), 94.5 (C-5), 94.3 (−OCH_2O−), 56.7 (−OCH_3), 56.5 (−OCH_3), 32.0 (CH_3−Ac). LCMS: r.t. = 1.01 min, *m/z* = 257.0 $[M+H]^+$.

Preparation of (*E*)-1-[2-hydroxy-4,6-bis(methoxymethoxy)phenyl]-3-phenylprop-2-en-1-one (9)

To a solution of 1-[2-hydroxy-4,6-bis(methoxymethoxy)phenyl]ethan-1-one (**8**, 0.277 g, 1.081 mmol) in 1,4-dioxane (3.10 mL), benzaldehyde (0.22 mL, 2.16 mmol, 2 eq.) was added. After stirring for 5 min at room temperature, an aqueous solution of NaOH 50 % (w/v) (3.10 mL) was added and the temperature was raised to 100 °C. The reaction was followed by LCMS and reached completion (95 % reaction yield) after stirring for 16 h. The mixture was cooled to room temperature, neutralized with HCl 2 M and stirred for 30 more min. It was then washed with water (1×10 mL) and extracted with EtOAc (3×10 mL). Once combined, the organic layers were dried over magnesium sulphate, filtered-off, concentrated under vacuum and purified by preparative HPLC to afford compound **9** as an orange solid; m.p. = 89–90 °C; ^{1}H NMR ($CDCl_3$) δ 13.81 (1H, s, OH-2′), 7.93 (1H, d, J_{trans} = 15.61 Hz, H-3, 7.79 (1H, d, J_{trans} = 15.63 Hz, H-2), 7.61 (2H, m, H-2″, H-6″), 7.41 (3H, m, H-3″, H-4″, H-5″), 6.32 (1H, d, J_{meta} = 2.20 Hz, H-3′), 6.25 (1H, d, J_{meta} = 2.32 Hz, H-5′), 5.29 (2H, s, −OCH_2O−), 5.19 (2H, s, −OCH_2O−), 3.54 (3H, s, −OCH_3) 3.49 (3H, s, −OCH_3); ^{13}C NMR δ 193.0 (C-1), 167.4 (C-2′), 163.5 (C-4′), 159.9 (C-6′), 142.5 (C-3), 135.0 (C-1″), 130.2 (C-2), 129.0 (C-3″, C-5″), 128.3 (C-2″,

C-6″), 127.4 (C-4″), 107.6 (C-1′), 95.2 (C-3′), 94.8 (C-5′), 94.1 (–O*C*H$_2$O–), 56.9 (–O*C*H$_3$), 56.5 (–O*C*H$_3$). LCMS: r.t. = 1.32 min, *m/z* = 345.0 $[M+H]^+$.

Preparation of 5,7-dihydroxyflavone (chrysin, 5)

To a solution of (*E*)-1-[2-hydroxy-4,6-bis(methoxymethoxy)phenyl]-3-phenyl-prop-2-en-1-one (**9**, 0.1 g, 0.29 mmol) in dry pyridine (8.5 mL), iodine (0.147 g, 0.58 mmol, 2 eq.) was added under N_2 atmosphere and the mixture was stirred at 110 °C. The reaction was followed by LCMS and the starting material was fully consumed after 16 h. The mixture was then cooled to room temperature, neutralized with HCl 2 M and then washed with a saturated solution of sodium thiosulfate. The mixture was extracted with DCM (3 × 20 mL), the organic layers were combined, dried over magnesium sulphate, filtered-off and concentrated under vacuum. The residue was then dissolved in ethanol (15 mL) and *p*-TsOH (50 mg, 0.29 mmol, 1 eq.) were added. The mixture was stirred under reflux and the reaction was followed by LCMS. After 20 h, the reaction had reached completion (81 % reaction yield). The mixture was cooled to room temperature, washed with water (1 × 15 mL) and extracted with DCM (5 × 20 mL). The organic layers were combined, dried over magnesium sulphate, filtered-off and concentrated under vacuum. The residue was purified by preparative HPLC to afford compound **5** as a yellowish solid; m.p. = 281–282 °C (lit. 275–276 °C [30]); ^{1}H NMR ($COCD_3$) δ 12.89 (1H, s, OH-5), 9.79 (1H, s, OH-7), 8.06 (2H, m, H-2′, H-6′), 7.60 (3H, m, H-3′, H-4′, H-5′), 6.78 (1H, s, H-3), 6.58 (1H, d, J_{meta} = 1.93 Hz, H-8), 6.28 (1H, d, J_{meta} = 1.92 Hz, H-6); ^{13}C NMR δ 183.2 (C-4), 165.2 (C-7), 164.7 (C-2), 163.4 (C-5), 159.0 (C-8a), 132.7 (C-4′), 132.3 (C-1′), 130.0 (C-3′, C-5′), 127.3 (C-2′, C-6′), 106.2 (C-3), 105.6 (C-4a), 99.9 (C-6), 94.9 (C-8). LCMS: r.t. = 0.73 min, *m/z* = 255.0 $[M+H]^+$.

Preparation of 5,7-dihydroxychromone (6)

To a solution of 1-[2-hydroxy-4,6-bis(methoxymethoxy)phenyl]ethan-1-one (**8**, 0.174 g, 0.68 mmol) in ethyl formate (5.55 mL), sodium hydride 60 % dispersion in mineral oil (0.160 mg), previously washed (three times) with isohexane, was added at 0 °C. The mixture was stirred at room temperature and the reaction was followed by LCMS. After 2.5 h the starting material was fully consumed and MeOH (3 mL) was added, followed by the addition of conc. HCl (0.1 mL). The temperature was raised to 40 °C, and the mixture was stirred for another 24 h. At this point, the reaction had reached completion, as detected by LCMS (91 % reaction yield). The mixture was then cooled to room temperature, poured into water and extracted with DCM (5 × 15 mL). The organic layers were combined, dried over magnesium sulphate, filtered-off and concentrated under vacuum. The residue was purified by column chromatography (isohexane/ethyl acetate 1:0→1:0), followed by preparative HPLC to afford the desired product **6** as white solid; m.p. = 274–277 °C (lit. 272–273 °C [31]); ^{1}H NMR (MeOD) δ 7.97 (1H, d, J_{cis} = 5.95 Hz, H-2), 6.34 (1H, d, J_{meta} = 2.08 Hz, H-8), 6.21 (1H, d, J_{meta} = 2.10 Hz, H-6), 6.19 (1H, d, J_{cis} = 5.96 Hz, H-3); ^{13}C NMR δ 183.4 (C-4), 166.2 (C-7), 163.5 (C-5), 159.9 (C-8a), 158.1 (C-2), 111.6 (C-3), 100.3 (C-6), 95.1 (C-8). LCMS: r.t. = 0.18 min, *m/z* = 178.8 $[M+H]^+$.

Recombinant expression and purification of amyloid beta ($A\beta_{1-42}$)

Recombinant $A\beta_{1-42}$ peptide was expressed in *Escherishia coli* BL21 Gold(DE3) strain and purified as described previously [32]. Briefly E. coli cells were sonicated and inclusion bodies were dissolved in M urea, ion exchange in batch mode on DEAE-cellulose resin was performed followed by liophilization. The lyophilized fractions were further dissolved in 6 M GuHCl and incubated 1 h at room temperature, then they were purified using a Superdex 75 HR 10/300 column (GE Healthcare) with 50 mM HEPES pH 7.4 and monomeric fraction was isolated.

Analysis of $A\beta_{1-42}$ aggregation kinetics

For the kinetic experiments the obtained $A\beta_{1-42}$ monomer was diluted to 3 μM and supplemented with ThT (6 μM) and 1 % of DMSO. All the samples were prepared in low-binding tubes (Axygen) on ice using careful pipetting to avoid introduction of air bubbles. It was used a 96-well half-area, low binding polyethylene glycol coating plate (Corning 3881) with a clear bottom. In all cases compounds were first solubilized in 100 % dimethyl sulfoxide (DMSO) solution to a concentration of 10 mM and then diluted to reach a final DMSO concentration of 1 %. Assays were performed at 37 °C under quiescent conditions in a plate reader (Fluostar Optima, BMG Labtech). The ThT fluorescence was measured through the bottom of the plate with a 440 nm excitation filter and a 480 nm emission filter. Each condition was followed in three wells. Compounds alone were tested as controls and do not interfere with ThT fluorescence. It is reported that additions up to 1 % of DMSO in the reaction mixture has no effect on $A\beta_{1-42}$ aggregation [10]. Amylofit online platform was used to analyze the ThT data and to determine the microscopic assembly processes. The analysis is based with primary and secondary nucleation processes occurring on the integrated rate laws describing the evolution of total fibril mass. Half-time of the transitions and the lag phase time were calculated as the time points at which 50 % and 10 % of the maximal ThT signal was reached, respectively. For all kinetics was used the model of secondary nucleation with primary reaction order $n_c = 2$ and secondary reaction order $n_2 = 2$.

AFM imaging

For the morphological characterization, Nanoscope IIIa multimode atomic force microscope produced by Digital Instruments (Veeco, Santa Barbara, CA, USA) was used. All measurements were carried out by intermittent mode (TappingMode™) AFM using etched silicon tips (Bruker, TESP-V2) with a resonance frequency of ~300 kHz at a scan rate of ~1.5 Hz. Samples used in the ThT fluorescence assay were taken from the microplates, directly deposited onto freshly cleaved mica (Agar scientific) surfaces (35 μL) and allowed to adsorb to the surface for 45 min. Samples were then rinsed with Mili-Q water and dried with pure N_2. All images were acquired in ambient conditions (20 °C) and section analysis was performed using Veeco NanoScope analysis software version 6.14R1.

Chemistry

(+)-Dihydroquercetin (**3**) was extracted from the knot wood zones of Siberian larch (*Larix sibirica*) [33] while quercetin (**1**), luteolin (**2**) and apigenin (**4**) were purchased by Sigma-Aldrich. A four-step synthesis of chrysin (**5**) was developed with 40 % overall yield. Diprotection of 2,4,6-trihydroxyacetophenone (**7**) with methoxymethyl (MOM) ether groups, in the presence of potassium carbonate, in acetone under reflux (Scheme 1) afforded compound **8**, whose reaction with benzaldehyde in a sodium hydroxide-promoted Claisen Schmidt aldol condensation gave the intermediate chalcone **9** in high yield. Then, using iodine in pyridine under reflux for the oxidative cyclization, followed by acid-promoted deprotection of the MOM groups, chrysin (**5**) was formed in 81 % yield.

Compound **8** also served as the phenolic precursor for the synthesis of 5,7-dihydroxychromone (**6**). On the basis of the procedure described by Liu and co-workers [34] for the synthesis of a dibenzylchromone, compound **8** was dissolved in ethyl formate at 0 °C, and sodium hydride was added to afford the 2-hydroxychroman-4-one intermediate. By adding concentrated hydrochloric acid and stirring the reaction mixture at 40 °C for 24 h, a one-pot dehydration and MOM deprotection resulted in the formation of 5,7-dihydroxychromone (**6**) in 91 % yield.

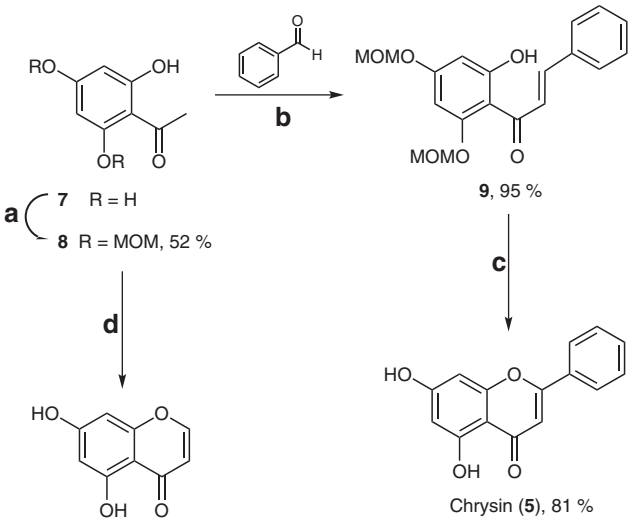

Scheme 1: Synthesis of chrysin (**5**) and 5,7-dihydroxychromone (**6**). Reagents and conditions: (a) acetone, K_2CO_3, chloromethyl methyl ether, reflux; (b) 1,4-dioxane, aq. NaOH 50 % (w/v), reflux; (c) (1) pyridine, I_2, reflux; (2) TsOH, MeOH, reflux; (d) (1) ethyl formate, NaH, 0 °C, (2) EtOH, (3) conc. HCl, reflux. Reaction yields were determined by LCMS.

Effects of flavonoids on Aβ aggregation kinetics

Following previous studies on the effects of flavonoids on Aβ aggregation [35], and seeking to establish a mechanistic basis of the effects of these compounds over aggregation pathways, we investigated the influence of flavonoids **1–5** and chromone **6** on Aβ aggregation. For this we monitored Aβ aggregation following thioflavin-T (ThT) fluorescence in the presence of each compound. We have used highly purified preparations of $Aβ_{1–42}$ [32] and carried out the aggregation kinetic experiments starting from homogenous preparations of monomeric $Aβ_{1–42}$ using well-defined protocols [36]. This approach yields highly reproducible kinetic data which allows reliable evaluation of the effects of the compounds studied on the $Aβ_{1–42}$ aggregation reaction (Fig. 3).

Observation of the kinetic traces of $Aβ_{1–42}$ aggregation at increasing compound concentrations up to a 30-fold molar excess allowed the observation of two different behaviors on the basis of total fibril mass formation, as inferred from the effect on the end-point ThT fluorescence intensity. As shown in Fig. 3d–f, apigenin (**4**), chrysin (**5**) and 5,7-dihydroxychromone (**6**) do not have a significant effect over $Aβ_{1–42}$ aggregation. In contrast, progressive decrease in the final ThT intensity is observed at increasing concentrations of quercetin (**1**), luteolin (**2**) and (+)-dihydroquercetin (**3**), which is indicative of a decrease in the total fibril mass by about 60 % at the highest tested concentrations (Fig. 4). Curve fitting of the kinetic traces allowed the determination of aggregation half times (mid-points of the sigmoidal transition) and aggregation lag times (time prior to the elongation stage) [37]. At 40 μM of compound concentration, we determined a relative decrease of up to 50 % in the lag time in the presence of quercetin (**1**), luteolin (**2**) and (+)-dihydroquercetin (**3**), an indication that in the presence of these compounds monomeric $Aβ_{1–42}$ needs less time to form primary aggregation nuclei [38].

Analysis of effects on microscopic mechanisms

We then carried out a quantitative analysis of the effect of the studied compounds over the microscopic reaction parameters. Data fitting of the aggregation reaction was analyzed using AmyloFit [39], that allows relating the macroscopic time evolution of the quantity of fibrils to the rate constants of different micro-

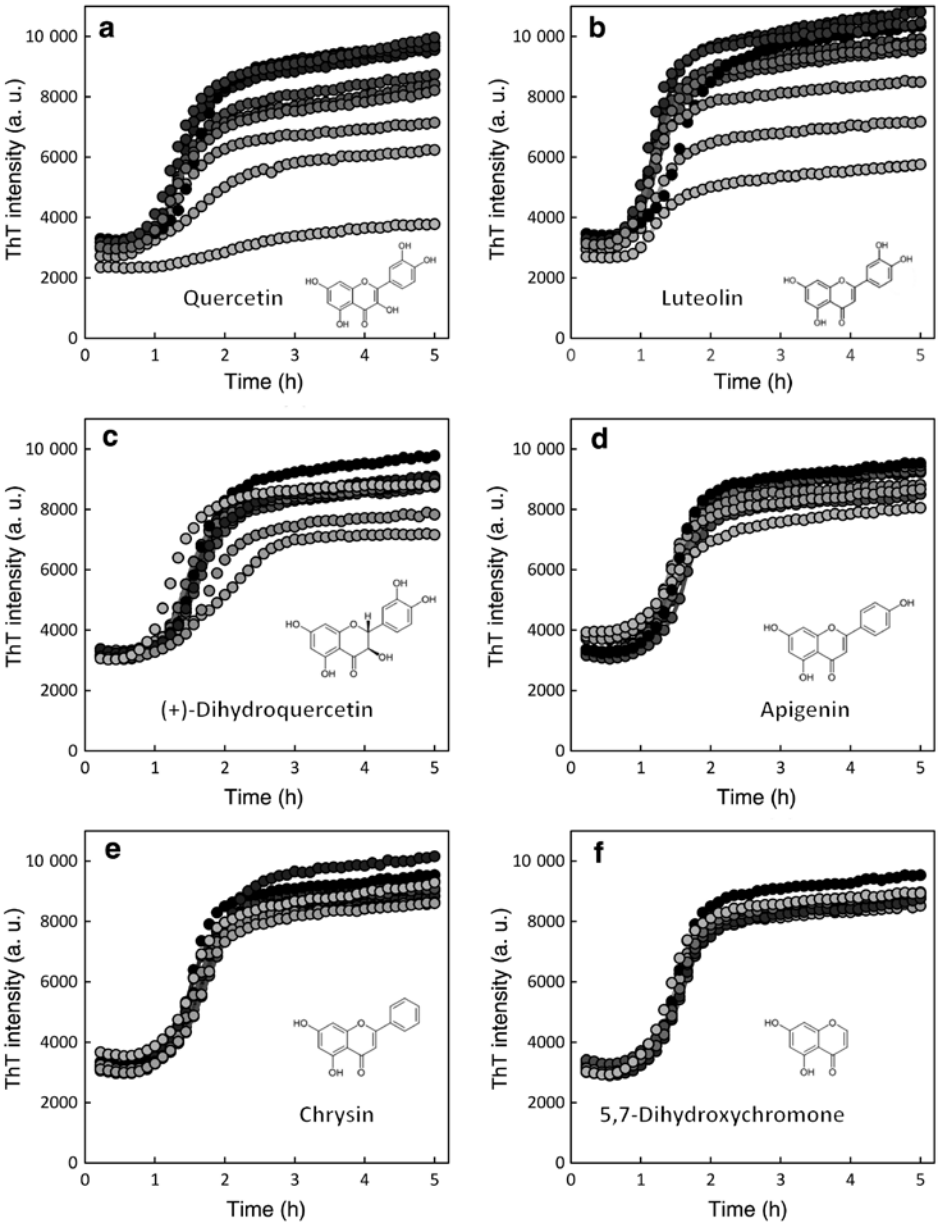

Fig. 3: Aggregation kinetics of $A\beta_{1-42}$ in the presence of compounds **1–6** at increasing molar ratios. Aggregation curves were obtained incubating $A\beta_{1-42}$ (3 μM, black dots) in 50 mM HEPES pH 7.4 + 1% DMSO at 37 °C and under quiescent conditions in the presence of 0.5, 1, 2.5, 5, 7.5, 10, 20, 40 and 100 μM of the different compounds (shown as a gradient from dark to lighter grey). (a) $A\beta_{1-42}$ + quercetin (**1**); (b) $A\beta_{1-42}$ + luteolin (**2**); (c) $A\beta_{1-42}$ + (+)-dihydroquercetin (**3**); (d) $A\beta_{1-42}$ + apigenin (**4**); (e) $A\beta_{1-42}$ + chrysin (**5**); (f) $A\beta_{1-42}$ + 5,7-dihydroxychromone (**6**). Plots represent averaged curved obtained from three independent replicates (n = 3) for each of the tested conditions.

scopic events involved in $A\beta_{1-42}$ aggregation (see Fig. 1). With this approach, the impact of the different molecules on the microscopic rates of the aggregation mechanism can be analysed, namely: primary nucleation rate (k_n), elongation rate (k_+) and secondary nucleation rate (k_2). All curves were normalized and fitted using a secondary nucleation dominated model, which is the established mechanism describing $A\beta_{1-42}$ aggregation [8]. We observed that none of the tested compounds affected the $A\beta_{1-42}$ aggregation mechanism, which remains unaltered as a secondary nucleation dominated process, in the presence of compounds in concentrations ranging from 0.5 to 100 μM. However, this kinetic analysis showed that some of the tested compounds can alter the relative contribution of the individual microscopic steps to the global

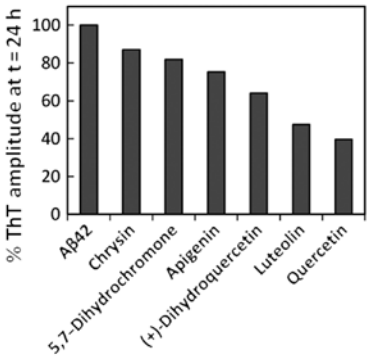

Fig. 4: $A\beta_{1-42}$ amyloid aggregate mass reduction by the effect of compounds **1–6**. The plot represents the relative fibril mass formed in the presence of each compound as inferred from the ThT amplitude measured at the plateau stage at the end point of the $A\beta_{1-42}$ aggregation reaction (t = 24 h) at the highest concentration tested for each compound (100 μM). The data shows the average over three replicates of each condition (n = 3).

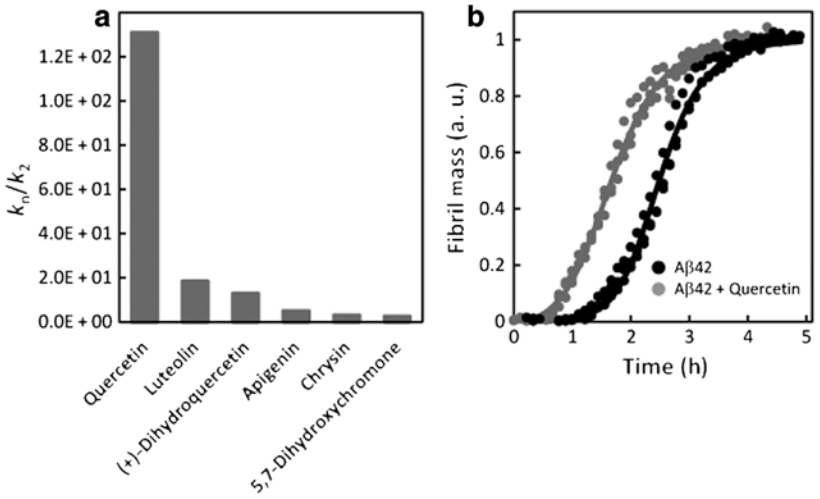

Fig. 5: Targeting primary nucleation of $A\beta_{1-42}$ aggregation. (a) Fitting of $A\beta_{1-42}$ aggregation (3 μM) in the presence of the studied compounds (40 μM) using a secondary nucleation model allowed determining effects over the ratio between primary and secondary nucleation rates for the different compounds. The represented ratios k_n/k_2 were normalized in respect to those determined in the absence of each compound. The k_2 rate has the same order of magnitude irrespective of the presence of any of the compounds. (b) Normalized time course for aggregation reactions of 3 μM $A\beta_{1-42}$ alone and in the presence of 40 μM quercetin (**1**) in 50 mM HEPES pH 7.4 + 1% DMSO at 37 °C and quiescent conditions. Each data point is the average of three independent replicates. The solid line represents the best fits for secondary nucleation with primary and secondary reactions order fixed at $n_c = n_2 = 2$.

aggregation mechanism. Comparison of the ratio between the primary nucleation (k_n) and secondary nucleation (k_2) rates allows to infer what is the microscopic process predominantly affected by each compound (Fig. 5a). This analysis showed that quercetin (**1**), luteolin (**2**) and (+)-dihydroquercetin (**3**) influence mostly the primary nucleation rate over effects on secondary processes. This is prominently illustrated in Fig. 5b which shows fitting of the aggregation curve of $A\beta_{1-42}$ (3 μM) in the presence of quercetin (40 μM). In the case of these three flavonoids, most prominently in the case of quercetin, this results in faster primary nucleation and decrease in lag time; since a decrease in fibril mass is detected, this may then be an indication that these compounds redirect the $A\beta_{1-42}$ aggregation towards off-pathway non-amyloidogenic oligomers (see Fig. 1), possibly by interacting with early primary $A\beta_{1-42}$ oligomers. Interestingly, it has been recently shown that both quercetin (**1**) and luteolin (**2**) are capable of binding to $A\beta_{1-40}$ primary oligomers as presumed from the incubation conditions (10 min incubation at 37 °C) leading to the formation of conformationally distinct species [37].

AFM topographic analysis

With the aim of complementing the results obtained from ThT fluorescence assays regarding the morphology of amyloid aggregates produced in the course of $A\beta_{1-42}$ self-assembly reaction, we then analysed the effect of each compound on $A\beta_{1-42}$ aggregation by AFM. As shown in Fig. 6, all compounds yielded distinct aggregates from those observed in the control sample (Fig. 6a), with a reduced number of the larger amyloid structures. In the particular case of quercetin (**1**, Fig. 6b) and luteolin (**3**, Fig. 6c), mica surfaces were much less populated.

Even though two discrete groups of compounds (catechol-type and non-catechol-type phenolic structures) could already be distinguished based on the results of ThT fluorescence assays, a wide variety of morphologies, fibril maturation states and aggregate distribution patterns were indeed observed. Samples at the aggregation end-points of ThT fluorescence assays and containing flavonoids and the synthesized chromone at the highest tested concentration (100 μM) were collected and directly applied onto mica surfaces for morphology analysis by AFM. At least two samples were prepared for each flavonoid and each surface was thoroughly analyzed. Regardless of the polymorphic aggregate distribution typically produced in the course of Aβ self-assembly reactions, all images presented are representative of the major features observed, as comparable distributions were observed on at least five different surface areas for each sample.

From a more detailed analysis of the control sample (3 μM of $A\beta_{1-42}$), two distinct types of morphologies could be distinguished: one containing fibrils ranging from ~6 nm up to ~20 nm in height (Fig. 7a and c) which constitute the major aggregate population, and another exhibiting elongated 1–2 nm high protofibrils with ~2–3 nm high oligomeric species (pointing arrows in Fig. 7b and d), forming strings of beads on the periphery of the denser aggregates previously described. These observations are consistent with the occurrence of secondary nucleation events involved in $A\beta_{1-42}$ aggregation (see Fig. 1), where thicker β-amyloid fibrils, which are not toxic by themselves in vivo, exhibit a surface-catalytic activity leading to the generation of diffusible toxic oligomers in the vicinity of amyloid plaques [8, 40]. As illustrated in Fig. 7b and d, these oligomeric species might be new on-pathway intermediates in fibril formation, thus feeding the positive feedback loop that assures a permanent source of new amyloid oligomers. In contrast with $A\beta_{1-42}$ protofibrils and fibrils, soluble amyloid oligomers are diffusible and readily available to destabilize neuronal cell membranes with consequent neuronal damage [41], thus raising the need to find active structures able to avoid the formation of the smaller oligomeric aggregates as a primary goal, instead of focusing on fibril formation or disruption.

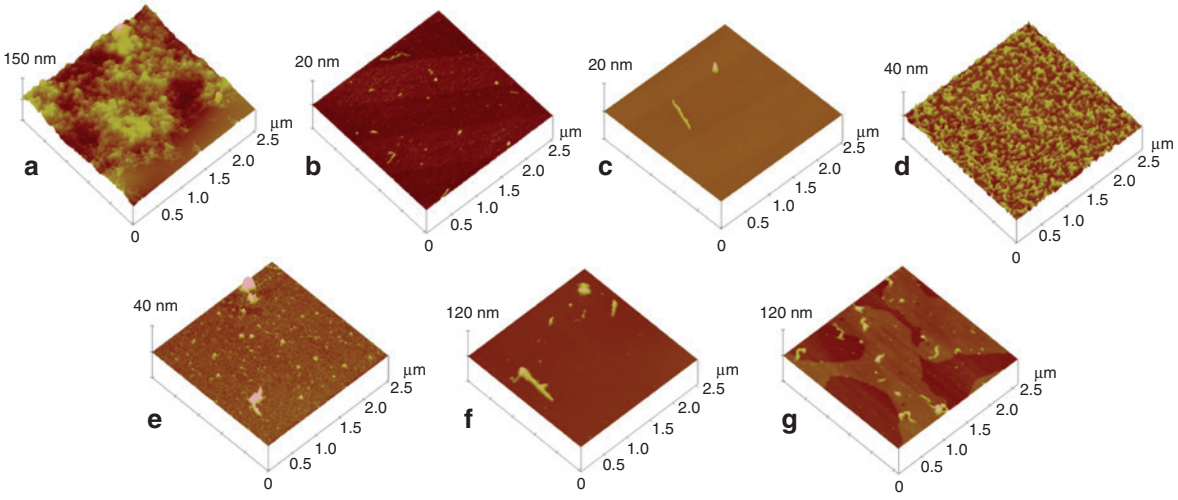

Fig. 6: Topographic analysis of $A\beta_{1-42}$ (3 μM) aggregates formed in the control sample (a) or in the presence of compounds **1–6** (100 μM) in 50 mM HEPES pH 7.4 + 1% DMSO by AFM (2.5 × 2.5 μm²): (b) $A\beta_{1-42}$ + quercetin (**1**); (c) $A\beta_{1-42}$ + luteolin (**2**); (d) $A\beta_{1-42}$ + (+)-dihydroquercetin (**3**); (e) $A\beta_{1-42}$ + apigenin (**4**); (f) $A\beta_{1-42}$ + chrysin (**5**); and (g) $A\beta_{1-42}$ + 5,7-dihydroxychromone (**6**).

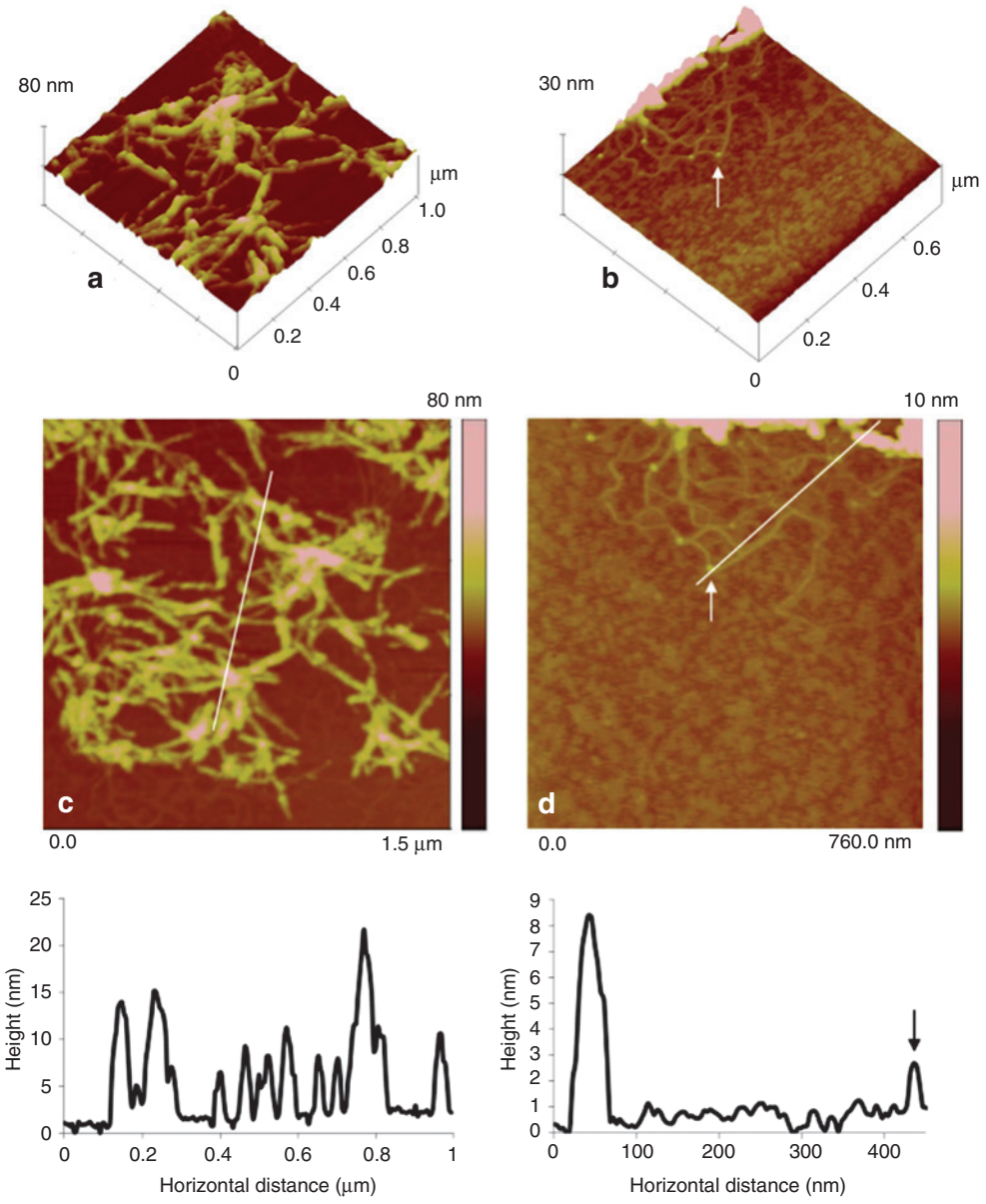

Fig. 7: Topographic analysis of fibrils, protofibrils and oligomers observed in the control sample (3 μM $A\beta_{1-42}$ in 50 mM HEPES pH 7.4 + 1% DMSO) by AFM. (a) 3D images of $A\beta_{1-42}$ fibrils (1 × 1 μm²); (b) 3D images of peripheral $A\beta_{1-42}$ protofibrils and oligomers (0.76 × 0.76 μm²); (c) 2D images and section analysis of $A\beta_{1-42}$ fibrils (z = 80 nm); (d) 2D images and section analysis of peripheral $A\beta_{1-42}$ protofibrils and oligomers (z = 10 nm).

Incubation of $A\beta_{1-42}$ with quercetin (**1**) promoted the conversion of $A\beta_{1-42}$ monomers into small and irregular fibrillary aggregates with an approximate height of 0.5–1.8 nm, together with spherical oligomeric structures ca. 0.5–1.25 nm high (Fig. 8a). Inspection of the mica surfaces by optical microscopy denotes that these are scarcely populated with virtually no aggregates visible after the rinsing step, in contrast with the control sample (not shown). In the presence of luteolin (**2**), an even lower aggregate population density throughout the mica surface was observed (Fig. 6c); yet, more mature and intertwined fibrillary species were often visible, with heights of ca. 4–7 nm (Fig. 8b). Nevertheless, spherical oligomers were barely detected which might be an indication that luteolin (**2**), as suggested by ThT aggregation kinetic analysis, may be rather promoting the formation of off-pathway aggregates that do not bind so effectively to the mica surface. According to previous reports, amorphous-type aggregates may exhibit more hydrophobic amino acid residues exposed

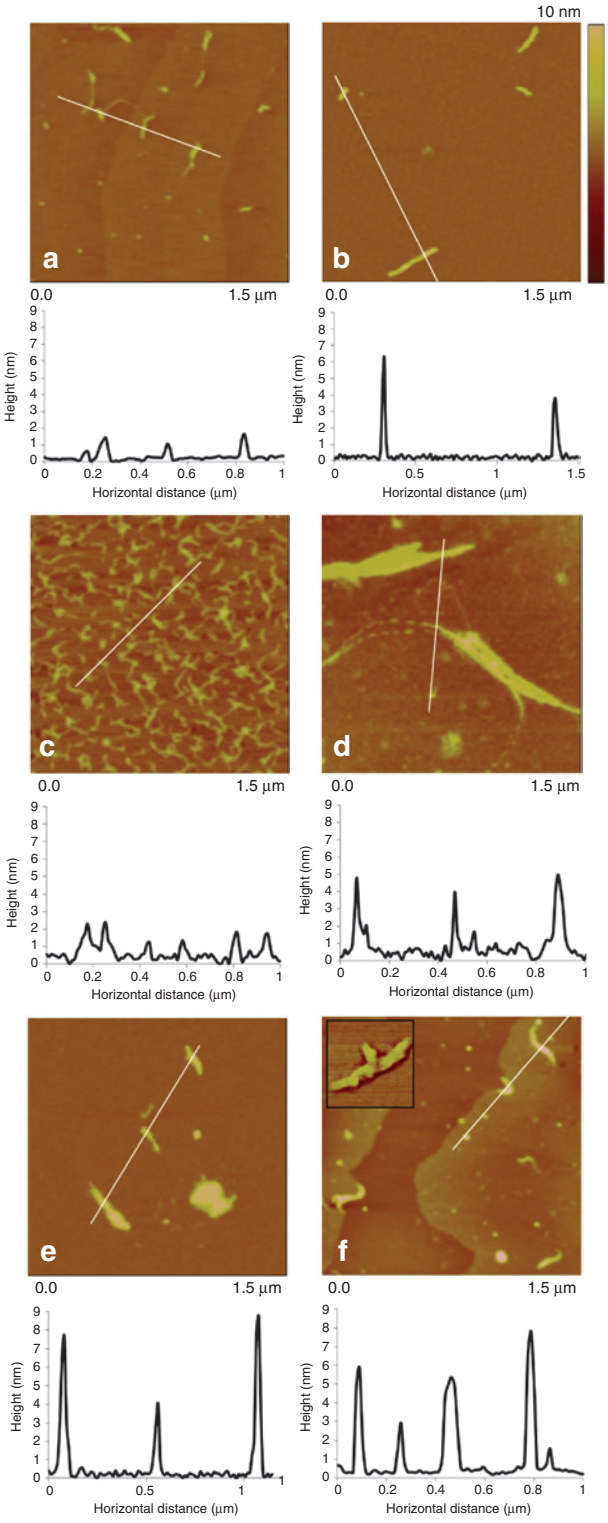

Fig. 8: Detailed topographic analysis of $A\beta_{1-42}$ (3 μM) aggregates formed in the presence of compounds **1–6** (100 μM) in 50 mM HEPES pH 7.4 + 1 % DMSO by AFM (z = 15 nm). (a) $A\beta_{1-42}$ + quercetin (**1**); (b) $A\beta_{1-42}$ + luteolin (**2**); (c) $A\beta_{1-42}$ + (+)-dihydroquercetin (**3**); (d) $A\beta_{1-42}$ + apigenin (**4**); (e) $A\beta_{1-42}$ + chrysin (**5**); and (f) $A\beta_{1-42}$ + 5,7-dihydroxychromone (**6**), phase image (inset): 0.215 × 0.215 μm².

at the surface than amyloid species, where these groups are known to be involved in β-sheet stacking [42, 43]. Thus, it is likely that off-pathway aggregates display less affinity to the mica surface which is negatively charged and, therefore, hydrophilic at neutral pH. Conversely, (+)-dihydroquercetin (**3**) shifted the formation

of $A\beta_{1-42}$ dense fibrillary aggregates into thin, ~1–2 nm high coil-shaped fibrils that homogeneously cover the entire mica surface (Fig. 8c and d). Spherical oligomers were seldom detected or indistinguishable from the vastness of fibrillary species observed, but those that were clearly identified had an average height of only 1.3–1.8 nm.

ThT fluorescence assays have shown that apigenin (**4**), chrysin (**5**) and 5,7-dihydroxychromone (**6**) (the non-catechol-type group of flavonoids in this study) do not significantly affect the evolution of total fibril mass when compared to the control sample. Indeed, clogged aggregates were visible on mica surfaces by optical microscopy (data not shown). The effect of apigenin (**4**) resulted into densely covered mica surfaces (Fig. 6e) displaying a multitude of small oligomers ca. 1–2 nm high, together with elongated protofibrils with heights up to ~5 nm. The latter species were frequently assembled together, forming aggregates with ~100–200 nm width (Fig. 8d). Aβ samples incubated with chrysin (**5**) exhibited much larger and more concentrated aggregates, individualized fibrils with heights ranging from ~4 nm up to ~9 nm shown in Fig. 8e, with the very sporadic occurrence of oligomeric structures ca. 2–3 nm high (Fig. 6f). In contrast, in the presence of 5,7-dihydrocromone (**6**) at least two populations of spherical oligomers spread all over the surface were clearly distinguished: a minor population comprising oligomers with an approximate height of ~6–8 nm, and a predominant population of oligomers with heights of ~1–2 nm (Fig. 8f). Moreover, shortened coil-shaped fibrils with ~6–9 nm in height were also detected, with phase images clearly showing semi-intertwined filaments composing these types of aggregates (inset of Fig. 8f). Hence, despite being densely populated (Fig. 6g), $A\beta_{1-42}$ samples containing non-catechol type flavonoids still display dramatic differences in composition and aggregate morphology when compared to the control sample.

Flavonoid structure variations: impact on Aβ aggregate morphology

The described association between significant reduction of total Aβ fibril mass and catechol-type flavonoids agrees with previous reports pointing towards catechol autoxidation as the underpinning cause for this effect [44]. Indeed, the so formed *o*-quinone is a Michael acceptor prone to react with protein lysine residues and has been regarded as an indispensable moiety for flavonoids to bind covalently to Aβ with a site-specific inhibitory mechanism in order to suppress its aggregation. Even though such observations suggest that targeting Aβ lysine residues could be an effective approach in the inhibition of β-amyloid aggregate formation, catechols have a high propensity for nonspecific reactions with other nucleophilic amino acid residues, namely cysteine and serine, being labelled as a Pan Assay Interference compoundS (PAINS) motif [45]. Hence, although active, the catechol-type compounds in this study merely allow the evaluation of the effect of two important flavonoid structural features: (a) the C2–C3 double bond and (b) the presence or absence of the hydroxy group in position 3. However, it seems that they are not a good choice for further optimization.

Anticipating the ability of quercetin (**1**) and (+)-dihydroquercetin (**2**) to inhibit $A\beta_{1-42}$ aggregation owing to the presence of the catechol moiety, we compared their effects in samples analysed by AFM, in order to understand the importance of the C2–C3 double bond, present in flavonols but absent in 3-hydroxyflavanones. A quite evident difference between samples containing each compound was observed (Fig. 8a vs. c). Indeed, a much more reduced amount of fibril-like aggregates was observed in the presence of quercetin (**1**) and oligomeric species generally displayed lower average heights (~0.5–1.5 nm) than those sparsely found in the presence of (+)-dihydroquercetin (**3**). However, while higher molecular weight monomers with heights over ~2–8 nm are the fibril-nucleating species of $A\beta_{1-42}$ [46], spherical oligomers with ~1–2 nm in height exhibit the greatest propensity to interact with phospholipidic vesicles and to induce neuronal necrosis at submicromolar concentrations when compared to 4–5 nm high oligomeric species [47]. Hence, even though quercetin (**1**) seems to be more effective at inhibiting the conversion of $A\beta_{1-42}$ monomers into fibril-like aggregates than its 3-hydroxyfavanone analogue, it still allows the generation of small spherical oligomers with neurotoxic potential. Moreover, our results only evidence occasional $A\beta_{1-42}$ oligomers on the mica surface in the presence of luteolin (**2**) when compared to samples containing quercetin (**1**) (Fig. 8b vs. a), thus opposing the need for the 3-OH in flavonoid analogues with optimized activity against $A\beta_{1-42}$ aggregation.

The contrasting effects of luteolin (**2**) and apigenin (**4**) over the $A\beta_{1-42}$ self-assembly reaction (Fig. 8d vs. e) observed throughout this study may be attributed to the presence of the catechol group in the first flavonoid. Yet, when compared to chrysin (**5**), apigenin (**4**) exhibited extensive networks composed by elongated protofibrils, which have been described as neurotoxic amyloid species [48]. Furthermore, samples containing apigenin (**4**), but not chrysin (**5**), presented widespread populations of small oligomers with 1–2 nm of height (Fig. 8d vs. e). Although we did not carry out toxicity studies, it is recognized that there is an inverse correlation between the size of Aβ assemblies and the potency of their exerted toxicity [48]. Larger $A\beta_{1-42}$ aggregates were detected in the presence of chrysin (**5**), suggesting our results that the 4′-OH group may be undesired in the flavone structure by stabilizing the formation of less mature amyloid species.

By conducting this research, we were interested in disclosing how far the flavonoid core could be simplified, yet retaining the desired activity against $A\beta_{1-42}$ aggregation. By comparing the effects of chrysin (**5**) and 5,7-dihydroxychromone (**6**) over the morphology of the generated amyloid aggregates, one can conjecture that the presence of ring B may be a structural requirement, as numerous types of aggregates were consistently observed by AFM throughout the mica surface of samples containing 5,7-dihydroxychromone (**6**), including small fibril-nucleating oligomeric species – which were only seldom detected in the presence of chrysin (**5**). This observation supports the generally-accepted hypothesis that π–π stacking interactions between aromatic amino acid side chains are on the basis of the amyloid self-assembly process, seemingly requiring the contribution of aromatic rings in small-molecule inhibitors for the disruption of their characteristic lamellar cross-β-sheet structures [49–51]. $A\beta_{1-42}$ aggregate morphology in the presence of 5,7-dihydroxychromone (**6**) is still very distinctive from that of the amyloid species present in the control sample, suggesting some level of affinity of this rather small structure towards the amyloid peptide.

Conclusions

Quercetin (**1**), luteolin (**2**) and (+)-dihydroquercetin (**3**), the three catechol-like flavonoids herein investigated using ThT-monitored kinetics, were shown to reduce $A\beta_{1-42}$ fibril content at the highest tested concentrations. We demonstrated that these compounds do not affect the rate of secondary nucleation processes that assure Aβ aggregates proliferation, but rather accelerate primary nucleation events responsible for the formation of early oligomers. Henceforth, we postulate that catechol-type flavonoids may potentiate the production of these primary amyloid aggregates which, once assembled, are partially redirected towards off-pathway non-amyloidogenic species. Based on previous reports [44, 45], we assume that this might occur via catechol autoxidation into *o*-quinones followed by covalent modification of lysine side chains. Although the catechol group is a well-described PAINS motif and thus should be avoided in structure optimization, these data encourage structural changes on the flavonoid core able to mimic this effect by interfering with key lysine residues non-covalently, thus safely remodelling intermediate amyloid oligomeric species into off-pathway aggregates. However, other key structure features are highly important, as revealed by AFM topographic analysis. Indeed, while small oligomers were still detected in $A\beta_{1-42}$ samples containing quercetin (**1**), in the presence of luteolin (**2**) these species were hardly observed, thus favouring the flavone-type structure over flavonols for further optimization.

To the best of our knowledge, this is the first report comparing the ability of flavonoids differing on the presence of the C2–C3 double bond to influence $A\beta_{1-42}$ aggregation. AFM images displayed visible differences between samples containing quercetin (**1**) and (+)-dihydroquercetin (**3**), and highlighted the importance of structural planarity for the activity of these types of compounds when it comes to the formation of amyloid fibrillary species. Given that many planar natural compounds have been regarded as non-specific membrane-interfering entities [45], planar flavonoid $A\beta_{1-42}$ aggregation inhibitors should be carefully evaluated in regard to this matter so as to avoid PAINS issues. Furthermore, while non-catechol type flavonoids did not significantly affect total $A\beta_{1-42}$ fibril content even at the highest tested concentrations, our topographical analysis suggests that ring B may be a relevant structural feature contributing to π–π stacking interactions between aromatic amino acids side chains of the polypeptide chain. In contrast, the *p*-hydroxyphenyl moiety

at C2 seems to be connected to the presence of small Aβ oligomers and protofibrils. Thus, their structural equivalents should be avoided in compound optimization.

In conclusion, the flavone core exhibited potential as a scaffold for chemical modifications in the search for flavonoid-based inhibitors of small $A\beta_{1-42}$ oligomers, which have higher neurotoxic potential when compared to amyloid fibrils or even oligomers with larger dimensions [41, 47]. These might include modifications in ring B to optimize non-covalent interactions with $A\beta_{1-42}$ lysine residues while avoiding the catechol group (a PAINS motif), as well as the synthesis of *O*- and *C*-glycosylated derivatives, which have the potential to increase compound water solubility and bioavailability. Indeed, with demonstrated neuroprotective effects through multitarget mechanisms of action [24–26], we herein posit that chrysin (**5**) may also be a suitable non-pains flavonoid scaffold for further optimization against $A\beta_{1-42}$ oligomer formation and, consequently, against $A\beta_{1-42}$-induced neuronal damage. In this report, we also present an expedient methodology for the synthesis of chrysin (**5**), which can be applied in the synthesis of flavone derivatives with therapeutic potential against AD.

Acknowledgments: The European Union is gratefully acknowledged for the support of the project entitled "Diagnostic and Drug Discovery Initiative for Alzheimer's Disease" (D3i4AD), FP7-PEOPLE-2013-IAPP, GA 612347. Dr. Magnus Walter and Dr. Teresa Man are also gratefully acknowledged for the supervision of Ana Marta Matos during her secondment to Eli Lilly laboratories at Erl Wood Manor, UK. Preparation of (+)-dihydroquercetin was supported by Russian Science Foundation (grant no. 14-50-00126). Bial Foundation is acknowledged through grant PT/FB/BL-2014-343 (to CMG), as well as Fundação para a Ciência e a Tecnologia for support through projects UID/Multi/0612/2013 (to CQB), UID/Multi/04046/2013 (to BioISI), PTDC/NEU-NMC/2138/2014 and IF/01046/2014 (to CMG), PTDC/BIM-MET/2115/2014, and for the PhD grants SFRH/BD/93170/2013 (to AMM) and SFRH/BD/101171/2014 (to JSC).

References

[1] Alzheimer's Association. *Alzheimers Dement.* **12**, 459 (2016).
[2] A. M. Matos, M. P. Macedo, A. P. Rauter. *Med. Res. Rev*. (2017), in press.
[3] F. Licastro, E. Porcellini. *Oncoscience* **3**, 135 (2016).
[4] J. Miklossy, P. L. McGeer. *Aging (Albany NY)* **8**, 575 (2016).
[5] M. E. Oskarsson, J. F. Paulsson, S. W. Schultz, M. Ingelsson, P. Westermark, G. T. Westermark. *Am. J. Pathol.* **185**, 834 (2015).
[6] D. K. Kumar, S. H. Choi, K. J. Washicosky, W. A. Eimer, S. Tucker, J. Ghofrani. *Sci. Transl. Med.* **8**, 340RA72 (2016).
[7] X. Zhan, B. Stamova, L. W. Jin, C. DeCarli, B. Phinney, F. R. *Sharp. Neurology* **87**, 2324 (2016).
[8] S. I. Cohen, S. Linse, L. M. Luheshi, E. Hellstrand, D. A. White, L. Rajah, D. E. Otzen, M. Vendruscolo, C. M. Dobson, T. P. Knowles. *Proc. Natl. Acad. Sci. USA* **110**, 9758 (2013).
[9] S. J. C. Lee, E. Nam, H. J. Lee, M. G. Savelieff, M. H. Lim. *Chem. Soc. Rev*. **46**, 310 (2017).
[10] J. Habchi, P. Arosio, M. Perni, A. R. Costa, M. Yagi-Utsumi, P. Joshi, S. Chia, S. I. Cohen, M. B. Muller, S. Linse, E. A. Nollen, C. M. Dobson, T. P. Knowles, M. Vendruscolo. *Sci. Adv.* **2**, e1501244 (2016).
[11] C. Gomes. *Curr. Top. Med. Chem*. **12**, 2460 (2012).
[12] S. M. Willför, M. O. Ahotupa, J. E. Hemming, M. H. T. Reunanen, P. C. Eklund, R. E. Sjoholm, C. S. E. Eckerman, S. P. Pohjamo, B. R. Holmbom. *J. Agric. Food Chem.* **51**, 7600 (2003).
[13] A. Y. Yashin, A. N. Vedenin, Y. I. Yashin, D. V. Yashunsky, N. E. Nifantiev, B. V. Nemzer. *Nutr. Food Sci.* **47**, 297 (2017).
[14] G. Loers, D. V. Yashunsky, N. E. Nifantiev, M. Schachner. *J. Nat. Prod.* **77**, 1554 (2014).
[15] A. M. Sabogal-Guáqueta, J. I. Muñoz-Manco, J. R. Ramírez-Pineda, M. Lamprea-Rodriguez, E. Osorio, G. P. Cardona-Gómez. *Neuropharmacology* **93**, 134 (2015).
[16] J. S. Choi, M. N. Islam, M. Y. Ali, Y. M. Kim, H. J. Park, H. S. Sohn, H. A. Jung. *Arch. Pharm. Res*. **37**, 1354 (2014).
[17] M. A. Ansari, H. M. Abdul, G. Joshi, W. O. Opii, D. A. Butterfield. *J. Nutr. Biochem*. **20**, 269 (2009).
[18] Y. Zhang, K. Igarashi, Y. Li. *Biosci. Biotechnol. Biochem*. **80**, 1580 (2016).
[19] F. S. Tsai, H. Y. Cheng, M. T. Hsieh, C. R. Wu, Y. C. Lin, W. H. Peng. *Am. J. Chin. Med*. **38**, 279 (2010).
[20] K. Jiménez-Aliaga, P. Bermejo-Bescós, J. Benedí, S. Martín-Aragón. *Life Sci.* **89**, 939 (2011).
[21] J. B. Wang, Y. M. Wang, C. M. Zeng. *Biochem. Biophys. Res. Commun.* **415**, 675 (2011).
[22] Y. R. Liao, J. Y. Lin. *Life Sci.* **137**, 89 (2015).

[23] L. Törmäkangas, P. Vuorela, E. Saario, M. Leinonen, P. Saikku, H. Vuorela H. *Biochem. Pharmacol*. **70**, 1222 (2005).
[24] S. F. Nabavi, N. Braidy, S. Habtemariam, I. E. Orhan, M. Daglia, A. Manayi, O. Gortzi, S. M. Nabavi. *Neurochem. Int.* **90**, 224 (2015).
[25] R. Mani, V. Natesan, R. Arumugam. *Biomed. Pharmacother*. **88**, 762 (2017).
[26] A. Vedagiri, S. Thangarajan. *Neuropeptides*. **58**, 111 (2016).
[27] H. M. El-Bassossy, S. M. Abo-Warda, A. Fahmy. *Am. J. Chin. Med*. **42**, 1153 (2014).
[28] H. X. Li, Z. C. Wang, Y. M. Qian, X. Q. Yan, Y. D. Lu, H. L. Zhu. *Chem. Biol. Drug Des.* **89**, 136 (2017).
[29] X. Wen, T. Walle. *Drug Metab. Dispos*. **34**, 1786 (2006).
[30] P. A. Kumar. *IJRAP*. **1**, 255 (2010).
[31] R. Pendse, A. V. R. Rao, K. Venkataraman. *Phytochemistry* **12**, 2033 (1973).
[32] D. M. Walsh, E. Thulin, A. M. Minogur, N. Gustavsson, E. Pang, D. B. Teplow, S. Linse. *FEBS J.* **276**, 1266 (2009).
[33] D. V. Yashunsky, V. M. Menrshov, D. E. Tsvetkov, Yu. E. Tsvetkov, A. A. Bel'ko, G. G. Vasiyarov, E. V. Titova, A. V. Pimenov, A. A. Onuchin, V. A. Dokichev, Yu. V. Tomilov, N. E. Nifantiev. *Russ. Chem. Bull. Int. Ed.* **63**, 2571 (2014).
[34] G. B. Liu, J. L. Xu, M. Geng, R. Xu, R. R. Hui, J. W. Zhao, Q. Xu, H. X. Xu, J. X. Li. *Bioorg. Med. Chem.* **18**, 2864 (2010).
[35] H. J. Lee, R. A. Kerr, K. J. Korshavn, J. Lee, J. Kang, A. Ramamoorthy, B. T. Ruotolo, M. H. Lim. *Inorg. Chem. Front.* **3**, 381 (2016).
[36] E. Hellstrand, B. Boland, D. M. Walsh, S. Linse. *ACS Chem. Neurosci.* **1**, 13 (2010).
[37] P. Arosio, M. Vendruscolo, C. M. Dobson, T. P. Knowles. *Trends Pharmacol. Sci*. **35**, 127 (2014).
[38] P. Arosio, T. P. Knowles, S. Linse. *Phys. Chem. Chem. Phys*. **17**, 7606 (2015).
[39] G. Meisl, J. B. Kirkegaard, P. Arosio, T. C. Michaels, M. Vendruscolo, C. M. Dobson, S. Linse, T. P. Knowles. *Nat. Protoc.* **11**, 252 (2016).
[40] T.L. Spires-Jones, M. L. Mielke, A. Rozkalne, M. Meyer-Luehmann, A. de Calignon, B.J. Bacskai, D. Schenk, B. T. Hyman. *Neurobiol. Dis*. **33**, 213 (2009).
[41] E. Evangelisti, R. Cascella, M. Becatti, G. Marrazza, C. M. Dobson, M. Setafi, C. Cecchi. *Sci. Rep*. **6**, 32721 (2016).
[42] R. Nelson, M. R. Sawaya, M. Balbirnie, A. Ø. Madsen, C. Riekel, R. Grothe, D. Eisenberg. *Nature* **435**, 773 (2005).
[43] D. Jiang, I. Rauda, S. Han, S. Chen, F. Zhou. *Langmuir* **28**, 12711 (2013).
[44] M. Sato, K. Murakami, M. Uno, Y. Nakagawa, S. Katayama, K. Akagi, Y. Masuda, K. Takegoshi, K. Irie. *J. Biol. Chem.* **288**, 23212 (2013).
[45] J. B. Baell. *J. Nat. Prod.* **79**, 616 (2016).
[46] I. A. Mastrangelo, M. Ahmed, T. Sato, W. Liu, C. Wang, P. Hough, S. O. Smith. *J. Mol. Biol.* **358**, 106 (2006).
[47] P. Cizas, R. Budvytyte, R. Morkuniene, R. Moldovan, M. Broccio, M. Lösche, G. Niaura, G. Valincius, V. Borutaite. *Arch. Biochem. Biophys*. **496**, 84 (2010).
[48] U. Sengupta, A. N. Nilson, R. Kayed. *EBioMedicine* **6**, 42 (2016).
[49] Y. Porat, A. Abramowitz, E. Gazit. *Chem. Biol. Drug. Des*. **67**, 27 (2006).
[50] E. Gazit. *FEBS J.* **272**, 5971 (2005).
[51] J. C. Sacchettini, J. W. Kelly. *Nat. Rev. Drug. Discov*. **1**, 267 (2002).